High-Speed Heterogeneous Data Acquisition using Martlet - A Next-Generation Wireless Sensing Node

Xinjun Dong, Shuo Chen, Dapeng Zhu, Michael Kane, Yang Wang, Jerome P. Lynch

Abstract— **This paper reports the latest development of a next-generation low-cost wireless sensing system for structural health monitoring, named Martlet. The Martlet sensing node design is based on a Texas Instruments Piccolo microcontroller, whose clock frequency is programmable up to 90 MHz. The high clock frequency of the microcontroller enables Martlet to support high-frequency data acquisition and high-speed onboard computation. The extensible design of the Martlet node conveniently allows incorporation of multiple sensor boards, so that structural response data can be simultaneously collected from a heterogeneous set of sensors. In this study, a strain gage sensor board is designed to be compatible for two common types of gages (120Ω and 350Ω). Besides anti-aliasing filter, selectable amplification gains are provided. In addition, an ultrasonic sensor board is developed to generate ultrasonic excitation signal and measure response signal, following a typical pitch-catch setup for detecting structural defects. The high-speed microcontroller on Martlet is able to collect the response signal at a high sampling rate of a few megahertz (MHz). Finally, an integrated accelerometer board is designed for low-cost acceleration measurement. The accelerometer board integrates a tri-axial MEMS (microelectromechanical system) accelerometer and associated signal conditioning circuits. One distinct feature of the signal conditioner is the on-the-fly programmable cut-off frequencies and amplification gains. Laboratory experiments are conducted to validate the performance of the Martlet wireless sensing system.**

I. INTRODUCTION

A nation's infrastructure is vital for economic, political and social development. Taking bridges for example, the United States has 607,751 bridges in operation in 2013 [1]. As bridges are continuously exposed to harsh outdoor environment and traffic loading, structural safety condition may deteriorate significantly throughout the designed service life. The latest ASCE 2013 report card shows that one in nine of the nation's bridges are rated as structurally deficient [2]. In order to improve the safety assessment of bridge, structural health monitoring (SHM) systems have been widely studied for monitoring structural performance and identifying potential damage. For example, weight-in-motion (WIM) technology is adopted to measure the structural response due to overloaded trucks [3-5]. Some other studies focus on crack development on structures, as crack growth in critical components may cause catastrophic bridge failure. One popular way of monitoring crack growth is to use solid ultrasonic wave for damage detection [6, 7]. Furthermore, many damage detection algorithms utilize the modal properties of a structure. Numerous approaches have been developed to obtain modal properties based on acceleration measurement from the structure [8, 9].

In general, various types of data are needed to evaluate the safety of a structure. In order to obtain more detailed structural information, it is required to install a large amount of sensors and data acquisition systems in the field. In traditional SHM systems, coaxial cable is usually adopted for data acquisition because of its reliable performance. However, coaxial cable has disadvantages such as high material cost and labor-intensive installation, which hinder extensive installation of cabled SHM systems [10]. In order to overcome the limitation of cabled SHM systems, significant efforts have been devoted to developing wireless SHM systems [11-14].

This paper reports the latest development of a next-generation, low-cost wireless sensing system for SHM, named Martlet [15]. The Martlet sensing node adopts a Texas Instruments Piccolo microcontroller to execute onboard computation and data acquisition. The dual-core architecture of the microcontroller enables parallel tasks to be simultaneously performed on the main core and a programmable control law accelerator (CLA) core. In addition, the 32-bit floating-point math accelerator on the CLA enables faster and more accurate onboard computation. The power-amplified wireless transducer on the Martlet node enables reliable communication up to 1,600 ft. An onboard Micro SD card reader provides additional memory for data storage. A variety of analog input channels are available allowing a large set of sensor boards to be interfaced with the Martlet node.

In this study, a strain gage board is developed for strain measurement with two common types of gages (120Ω and 350Ω). Furthermore, an ultrasonic board is designed to both generate and receive ultrasonic signals for nondestructive evaluation (NDE) on critical members of a structure. Finally, an accelerometer board is developed, integrating a tri-axial MEMS

Xinjun Dong, Shuo Chen, Dapeng Zhu and Yang Wang are with the School of Civil and Environmental Engineering, Georgia Institute of Technology, Atlanta, GA 30332 USA (corresponding author: Yang Wang. email : yang.wang@ce.gatech.edu; phone: +1(404) 894-1851; fax: +1(404)385-0337).
Jerome P. Lynch is with the Department of Civil and Environmental Engineering, University of Michigan.
Michael Kane is with the US Department of Energy's Advanced Research Project Agency-Energy (ARPA-E) in Washington, D.C.

(microelectromechanical system) accelerometer and associated signal conditioning circuit for low-cost acceleration measurement. The cut-off frequencies and amplification gains of the signal conditioning circuit can be programmed on the fly. The rest of this paper is organized as follows. Section II introduces the hardware design of the wireless sensing devices, including the Martlet node and three sensor boards (strain, ultrasonic and accelerometer boards). Section III describes performance evaluation of the wireless sensing system through laboratory experiments. Finally, a summary and discussion are provided.

II. DEVELOPMENT OF MARTLET WIRELESS SENSING DEVICES

This section describes the design and development of the Martlet wireless sensing system. The section first presents overall design of the Martlet sensing device. The development of three Martlet accessory sensor boards is then introduced, including the strain, ultrasonic, and accelerometer boards.

A. Martlet development

Martlet, as shown in Figure 1, is a next-generation low-cost wireless sensing node developed for smart structures applications [15]. The development of Martlet is a joint effort among the Laboratory for Intelligent Systems and Technologies at the University of Michigan, the Laboratory for Smart Structural Systems at Georgia Institute of Technology, and the Department of Civil and Environmental Engineering at Michigan Technological University. The Martlet wireless node adopts a Texas Instruments Piccolo microcontroller as the core processor. An earlier version (TMX320F28069) of the microcontroller supports programmable clock frequency up to 80 MHz, and the later version (TMS320F28069) supports up to 90 MHz.

One key feature of the Martlet node is its extensible hardware design, which enables various sensor boards to easily stack up through four connectors and work with the motherboard. Integrating the extensible design feature with onboard 9-channel 12-bit analog-to-digital conversion (ADC), the Martlet node is able to simultaneously sample analog signals from multiple sensors through different accessory sensor boards (termed "wing" boards). In addition, various general purpose input/output (GPIO) pins are extended to the wing connectors, which allow communication between the microcontroller and peripheral components using protocols such as serial peripheral interface (SPI), inter-integrated circuit (I^2C), and pulse width modulation (PWM), etc. The microcontroller also has 100 kB × 16-bit random access memory (RAM) for embedded computing. To store large quantity of data, a typical Micro SD card (like these used in digital cameras) can be plugged into the motherboard. The data stored in the Micro SD card can be either wirelessly transferred or easily read offline by a personal computer. The Martlet node integrates a 2.4GHz radio for low-power wireless communication through IEEE 802.15.4 standard [16]. The communication range can be up to 1,600 ft at line-of-sight, and the maximum transfer rate can reach 250 kbps.

The high clock frequency of the microcontroller enables the Martlet node to execute high-speed data acquisition and onboard computation. The capability of high-speed data processing enables the Martlet node to generate kHz or MHz ultrasonic bursts for nondestructive evaluation (NDE). The direct memory access (DMA) module on the microcontroller allows the Martlet node to sample data at a frequency up to 3 MHz, which is sufficient for capturing ultrasonic signals. The dimension of the Martlet node is 2.5 in by 2.25 in.
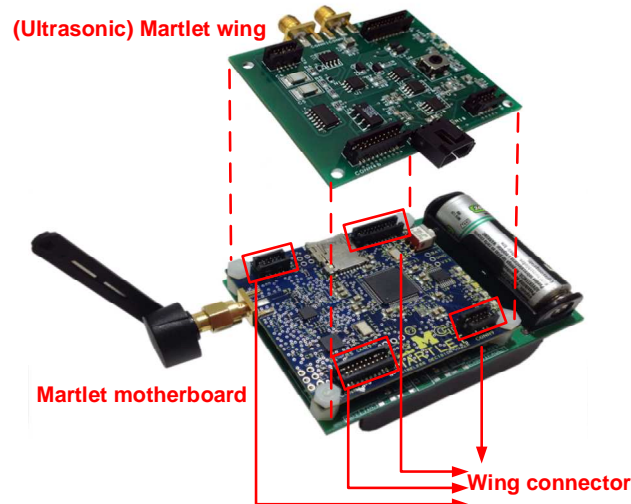

Figure 1. The Martlet wireless node with wing connectors (2.5 in × 2.25 in)

B. Strain gage wing board

In order to incorporate strain measurement into the Martlet wireless sensing system, a strain gage wing is developed (Figure 2). The strain gage wing is compatible with two types of commonly-used strain gages (120Ω and 350Ω). A total of three strain gages can be connected with each strain gage wing. The functional diagram of the strain gage wing is shown in Figure 3. Each strain gage channel of the wing provides three major functions, i.e. quarter Wheatstone bridge circuit, signal amplification, and anti-aliasing filtering.

The quarter Wheatstone bridge is used to convert the resistance value of a strain gage into a voltage signal (changing with strain) as output of the bridge circuit. An onboard jumper allows selection of the strain gage type (120Ω or 350Ω). Since the deformation of many engineering structures is usually small (e.g. at tens of microstrains), without amplification, the variation in output voltage signal is low and can be easily contaminated by electrical noise. To overcome this difficulty, an amplification circuit, using an instrumentation amplifier, is designed to increase the signal-to-noise ratio.

Another onboard jumper allows the selection of the amplification gain (×477 or ×96). The amplification gain also determines the measurement range of the strain gage wing, which is ±2,000με for ×477 gain and ±10,000με for ×96 gain. Another function of the instrumentation amplifier is to shift the mean value of the voltage signal. At reference/zero strain, by using a thumbwheel potentiometer, the output voltage signal is shifted to the center of the Martlet ADC range (i.e. 1.65V) in order to achieve maximum measurement range for both positive and negative strains. Voltage fluctuation with respect to the reference voltage (1.65V) indicates strain change. Finally, the voltage signal goes through an anti-aliasing filter with a cutoff frequency of 25Hz to further reduce noise contamination. For backward compatibility, Molex connectors are provided so that the strain gage wing can also be interfaced with Narada, a previous generation of wireless sensing node [14] .
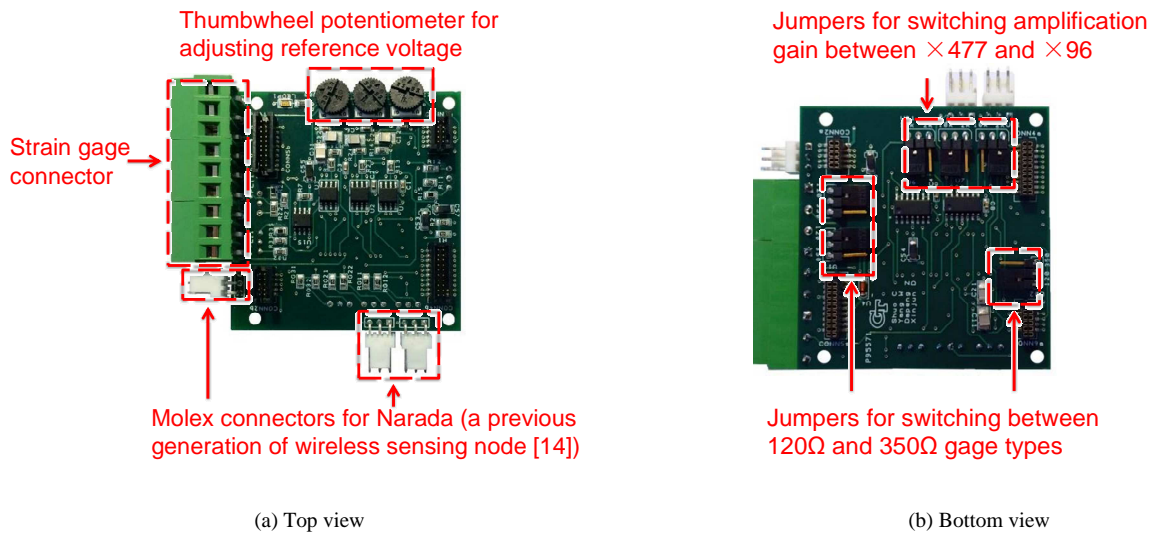

(a) Top view   (b) Bottom view

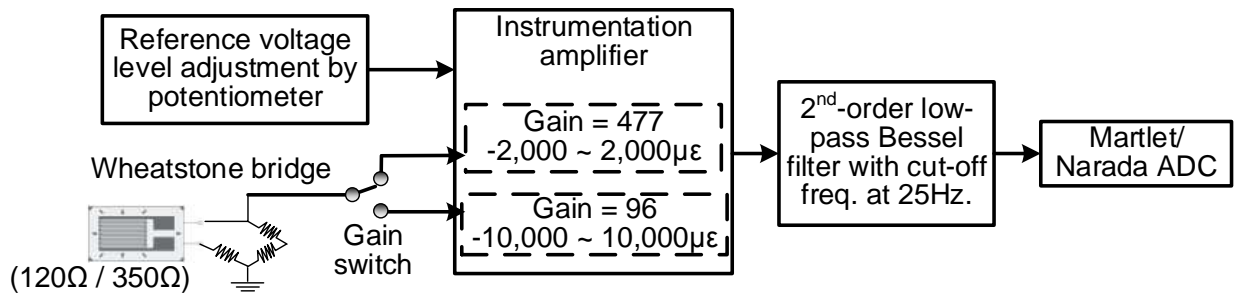Figure 2. The Martlet strain gage wing (2.5 in × 2.375 in)

Figure 3. Functional diagram of one channel in the strain gage wing

C. Ultrasonic wing board

Ultrasonic NDE is widely used for detecting crack development in structures. Through SMA connectors, the ultrasonic wing (Figure 4) can be interfaced with two commercial Ultran Group WC50-0.5 narrowband ultrasonic transducers (one transmitting and one receiving) to effectively detect crack growth with a typical pitch-catch setup. Center frequency of the transducer is 500 kHz. Figure 5 shows the functional diagram of the ultrasonic wing, which consists of an excitation module and a receiving module.

The excitation module provides excitation signal for the transmitting transducer, in order to generate ultrasonic waves into a structural surface. In this implementation, the Martlet node generates PWM bursts, each burst containing five cycles of square waves (0~3.3V) at 500 kHz frequency. Since the amplitude of ultrasonic wave decays rapidly during propagation, the transmitting transducer needs relatively high excitation voltage in order to generate clear response signals. To this end, the excitation module amplifies the square waves to ±9V while maintaining the 500 kHz frequency, and feeds the signal into the transmitting transducer. Using a plexiglass wedge, the transducer then launches a series of Rayleigh waves into structural surface[17].

After the Rayleigh wave propagates for a short distance, the receiving transducer captures the response signal and generates a zero-mean voltage output to the receiving module of the ultrasonic wing. The receiving module consists of three main functions, i.e. mean shifting, signal amplification, and anti-aliasing filter. The mean value of the output signal from the receiving module is uplifted to the center of Martlet ADC range (i.e. 1.65V). Since the immediately received signal at the transducer is of very low amplitude (~50mV), the signal needs to be amplified in order to increase the signal-to-noise ratio. The gain of the amplification module can be easily adjusted to 10dB, 20dB or 30dB by a rotary switch on the board. Finally, the received signal is processed by an anti-aliasing filter before entering the ADC module of the Martlet motherboard. If a crack exists between the transmitting and receiving sides, the magnitude of the received signal usually decreases with the increase of crack size. In order to capture the received signal with a center frequency of 500 kHz, the ADC sampling frequency should be at least 1 MHz to avoid aliasing. The direct memory access module in the Martlet microcontroller is used to implement 2.67 MHz sampling frequency, with the microcontroller clock set at 80 MHz.
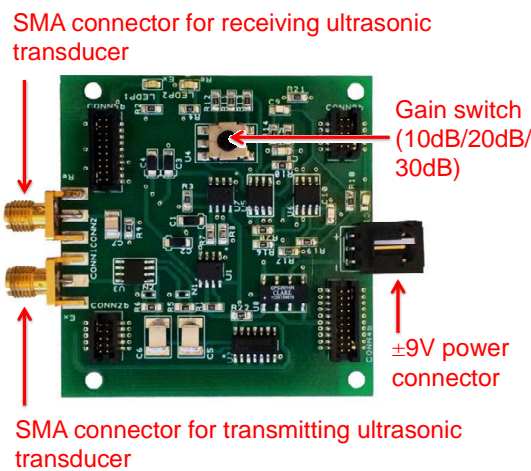

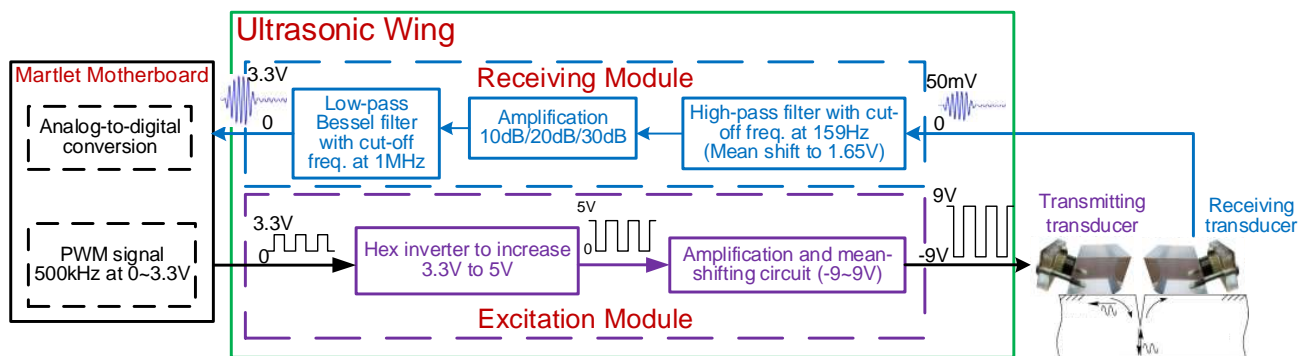Figure 4. The Martlet ultrasonic wing (2.5 in × 2.375 in)

Figure 5. Functional diagram of ultrasonic wing

D. Integrated accelerometer wing board

In order to obtain accurate acceleration measurement, and in the meantime reduce hardware cost, one solution is to integrate a low-cost MEMS accelerometer and specialized signal conditioning circuit into a single wing board, as shown in Figure 6(a). The integrated accelerometer wing adopts a tri-axial MEMS accelerometer, the ST Microelectronics LIS344ALH model. A jumper on the board selects between ±2g and ±6g measurement scales. The noise density of the measurement is 25 $\mu g / \sqrt{Hz}$ along the x-axis and y-axis, and 50 $\mu g / \sqrt{Hz}$ along the z-axis.

The analog signals from the LIS344ALH accelerometer are directly fed into an onboard signal conditioner that performs mean shifting, low-pass filtering, and amplification (Figure 7). The mean shifting module is particularly useful because the zero-g output voltage signals from the LIS344ALH accelerometer depend on the orientation of the accelerometer mount. Regardless of zero-g voltage levels of the sensor signals, the mean-shifted signals oscillate around 1.65V and the dynamic waveform remains the same as prior to shifting. Next, the anti-aliasing module prevents high-frequency signals and noises from irreversibly contaminating the digitalized data samples. A 4th-order low-pass Bessel filter with a programmable cutoff frequency is adopted in this anti-aliasing design. The phase shift of a Bessel filter varies linearly with frequency. This is equivalent to a constant time delay to the signal within the passband, and thus, preserves the original waveform [18]. The low-pass cut-off frequency can be programed on-the-fly from 15Hz to a few hundred hertz. In order to improve signal-to-noise ratio, the accelerometer signal is finally amplified by a programmable amplifier. The overall amplification gain can be set from ×1.9 to ×190. As noted, a distinct feature of the integrated accelerometer wing is that the cutoff frequencies and gains are remotely programmable. This feature is achieved by adopting digital potentiometers (Digipots), whose resistance value can be programed on-the-fly through an I^{2}C interface from the Martlet microcontroller. The programmable cutoff frequencies and gains offer great convenience in field testing. When a new set of cutoff frequencies and gains is needed, a wireless command from the server can easily achieve immediate setting update for all Martlet nodes.

The integrated accelerometer wing is placed into a compact weatherproof enclosure with a dimension of 2.28in (L) × 2.52in (W) × 1.38in (H), for firm installation of the accelerometer onto a structural surface (Figure 6(b)). Therefore, the wing is not stacked up to the Martlet motherboard. Rather, the integrated accelerometer wing is connected to the Martlet node with an eight-wire cable. Three wires in the cable are allocated for the acceleration output signals (X, Y and Z channels), two are allocated for I^{2}C communication, one is allocated for power, one is allocated for ground, and the last one is allocated to a digital signal that allows the Martlet motherboard to power the accelerometer wing on and off. The current consumption of the integrated accelerometer wing is ~12 mA (referenced at 3.3 V) under normal working conditions and ~1 μA when powered off into sleep mode.

(a) Integrated accelerometer wing (2.0 in × 2.25 in)   (b) Weatherproof package (2.28 in × 2.52 in × 1.38 in)
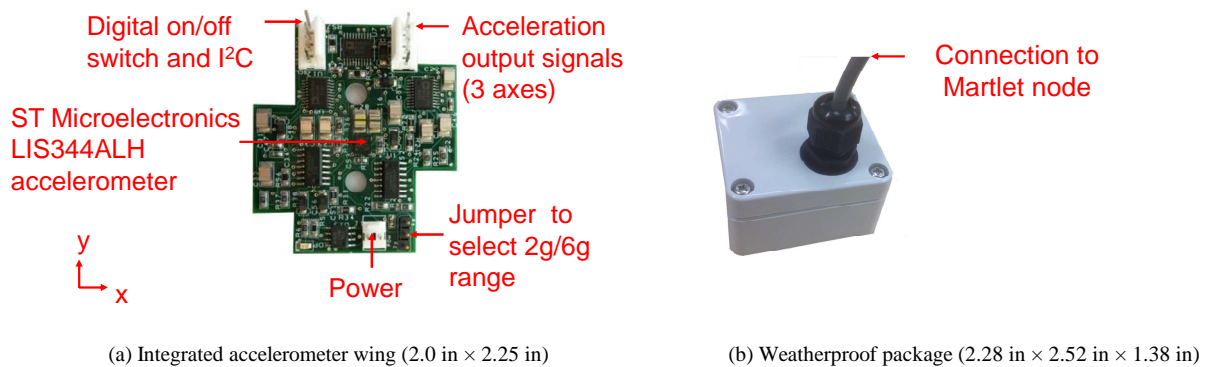
Figure 6. Integrated accelerometer wing with weatherproof package
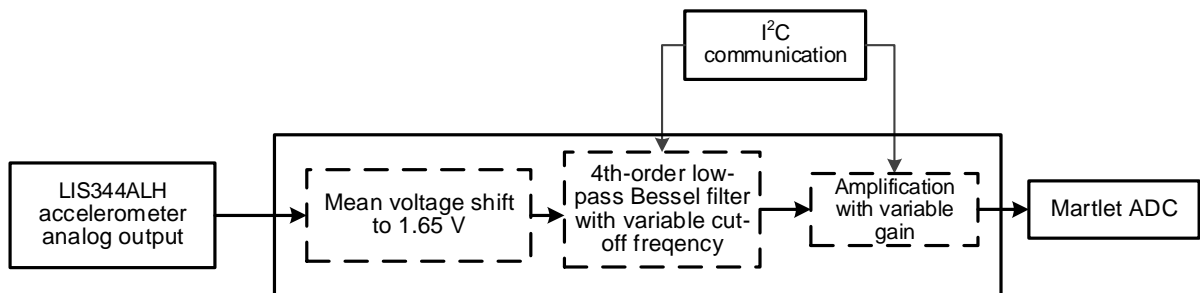

Figure 7. Functional diagram of integrated accelerometer wing

III. VALIDATION OF THE MARTLET WIRELESS SENSING SYSTEM

In order to evaluate the performance of the Martlet wireless node and the associated wings, laboratory experiments are conducted. Experiments are carried out with the strain gage wing for calibrating sensitivity value and quantifying noise level. The ultrasonic wing is tested with a notch specimen to evaluate its performance for defect detection. Finally, measurement of the integrated accelerometer wing is compared with that of a high-precision cabled accelerometer.

A. Validation of Martlet Strain Gage Wing

To assess the performance of the strain gage wing, two experiments are carried out. The first experiment calibrates the strain gage wing with a strain calibrator, and the second experiment assesses the noise level of the strain gage wing. The layout of the calibration experiment is shown in Figure 8. The quarter bridge setting of a commercial strain indicator calibrator (Vishay 1550A) is used to assess the measurement accuracy of the stain gage wing. Four scenarios of the strain gage wing are tested. Each scenario is a different combination of strain gage type and measurement range, including 120Ω with 2,000με range, 120Ω with 10,000με range, 350Ω with 2,000με range, and 350Ω with 10,000με range. For each scenario, data at six strain levels are collected and compared to the corresponding benchmark strain values of the calibrator. Figure 9 plots the strain measured by the strain gage wing against the benchmark strain value provided by the calibrator. A close match can be observed between two sets of strain data. Linear regression is performed between the two strain data sets, for each experiment scenario. The coefficient of determination (R^2) is calculated for each experiment scenario and shown in Figure 9, which demonstrates a high linearity between measured and benchmark values. Based on the output voltage of the strain gage wing (V_{out}) and benchmark strain value (V_{ref}), sensitivity of the strain gage wing can be calculated as:

$$S_{exp} = \frac{V_{out} - V_{ref}}{\varepsilon_{benchmark}} \tag{1}$$

where S_{exp} denotes the experimental sensitivity of the strain gage wing; $\varepsilon_{benchmark}$ represents the benchmark strain value. Taking 120Ω gage setting as an example, the results show that the experimental sensitivity is 0.7728mV/με for 2,000με range, and 0.1542 mV/με for 10,000με range.

The setup for noise level experiment is shown in Figure 10. The strain gage is free of external load and directly connected with a Martlet strain gage wing. Same as the calibration experiment, four scenarios are tested, each scenario with a different combination of gage type and measurement range. The sampling frequency is set as 100Hz, and sampling time is 10s. Figure 11 plots the measurement results of all four scenarios. The noise level in each experiment scenario is estimated by the standard deviation value (STD):

$$STD = \sqrt{\frac{1}{N-1} \sum_{i=1}^{N} (\Delta \varepsilon_i)^2} \tag{2}$$

where $\Delta \varepsilon_i$ denotes the difference between the ith strain value of the data set and the mean strain level; N is the total number of data points. Particularly for the two scenarios with 2,000με range, the noise level is only slightly over 1με, showing a performance comparable to cabled strain measurement systems. The noise level with 2,000με range (i.e. ×477 amplification gain) is lower than
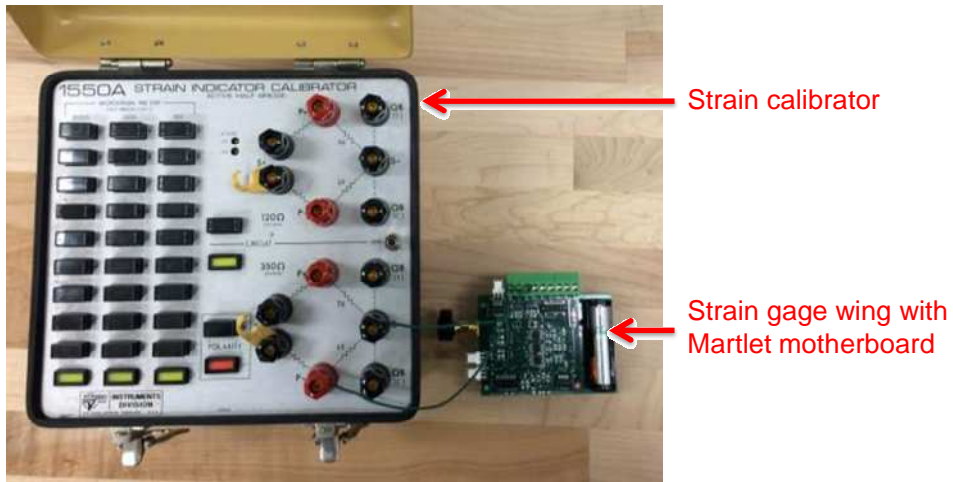

Figure 8. Calibration setup for strain gage wing

(a) 120Ω gage with 2,000 με range

(b) 350Ω gage with 2,000 με range

(c) 120Ω gage with 10,000 με range
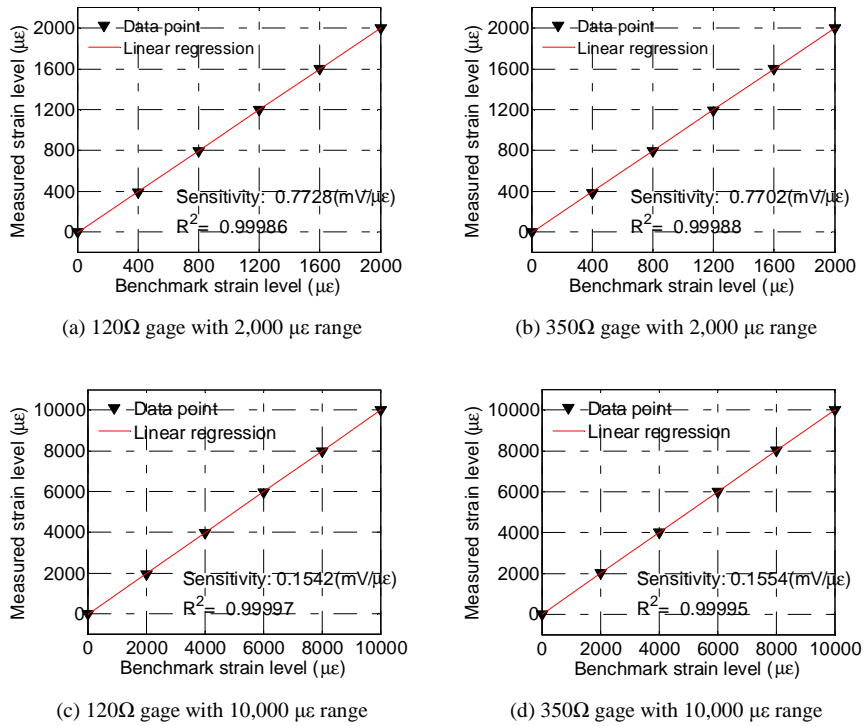
(d) 350Ω gage with 10,000 με range

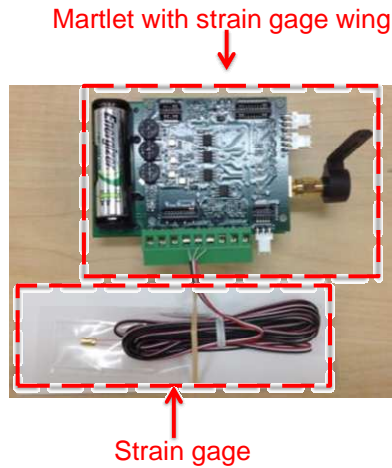Figure 9. Calibration results of the strain gage wing

Figure 10. Experiment setup for quantifying noise levels of the strain gage wing

that with 10,000με range (×96), which means that increase in the amplification gain can achieve better signal-to-noise ratio. Overall, both the calibration experiment and the noise level experiment demonstrate that the strain gage wing can accurately capture strain gage data.
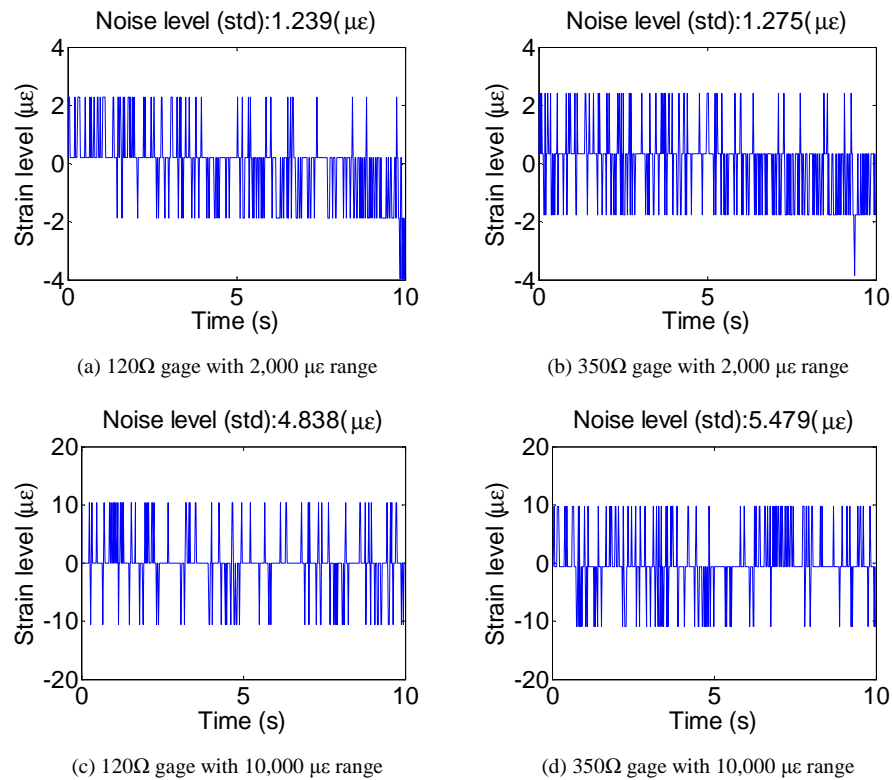
(a) 120Ω gage with 2,000 με range   (b) 350Ω gage with 2,000 με range

(c) 120Ω gage with 10,000 με range   (d) 350Ω gage with 10,000 με range

Figure 11. Noise level results of the strain gage wing
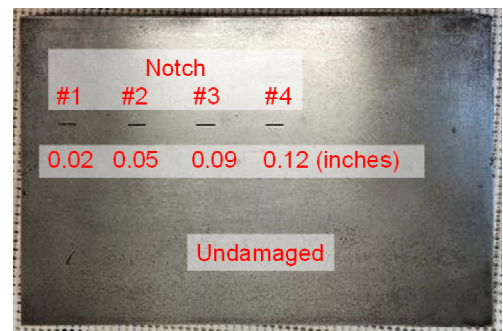
B. *Validation of ultrasonic wing*

In order to evaluate the effectiveness of the ultrasonic wing for monitoring crack, an experiment is carried out on a steel specimen (Figure 12(a)). There are four existing notches of different depths on the specimen surface, to simulate different levels of crack (Figure 12(b)). Using two wedge transducers, the pitch-catch ultrasonic data is collected on undamaged surface first and then across each notch. The high-speed microcontroller in the Martlet node enables high-frequency data acquisition. During the experiment, the sampling frequency is set as $f_s = 2$ MHz and, the gain is set as 30dB. Usually, the magnitude of the received signal decreases with a deeper notch.

The received signals are reconstructed to 200MHz sampling frequency, so as to better evaluate the magnitude of the received signal. The upper plot in Figure 13(a) shows the received signal for 60 ultrasonic bursts collected by the Martlet node. Each burst is generated by five cycles of 500 kHz square waves applied to the transmitting transducer. The excitation for each burst lasts for 10 µs, and the ultrasonic wave propagation response to each burst is collected for 260 µs at the receiving transducer, allowing the response to die out. The lower plot in Figure 13 (a) shows reconstructed signal, which demonstrates more consistent peak amplitude among bursts. In Figure 13(b), the reconstructed signal from one ultrasonic burst is compared with the signal collected by a cabled data acquisition system. Close match can be observed between two sets of signals. Therefore, it can be concluded that the signal reconstruction process can restore more authentic amplitude of the response signal.
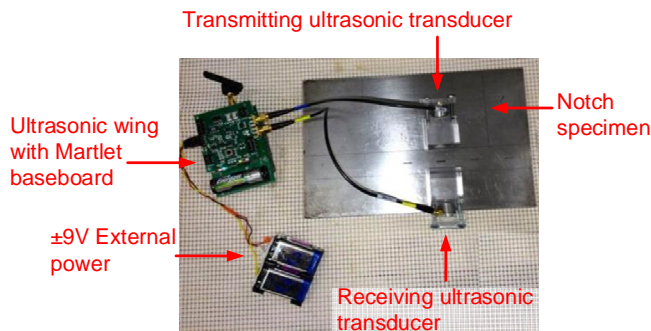
(a) Photo of the complete setup   (b) Photo of the specimen with four notches; notch depths are shown in inches

Figure 12. Experiment setup for the ultrasonic wing

(a) Comparison between original and reconstructed signals

(b) Comparison between reconstructed and cabled signals

(c) Envelope through HHT

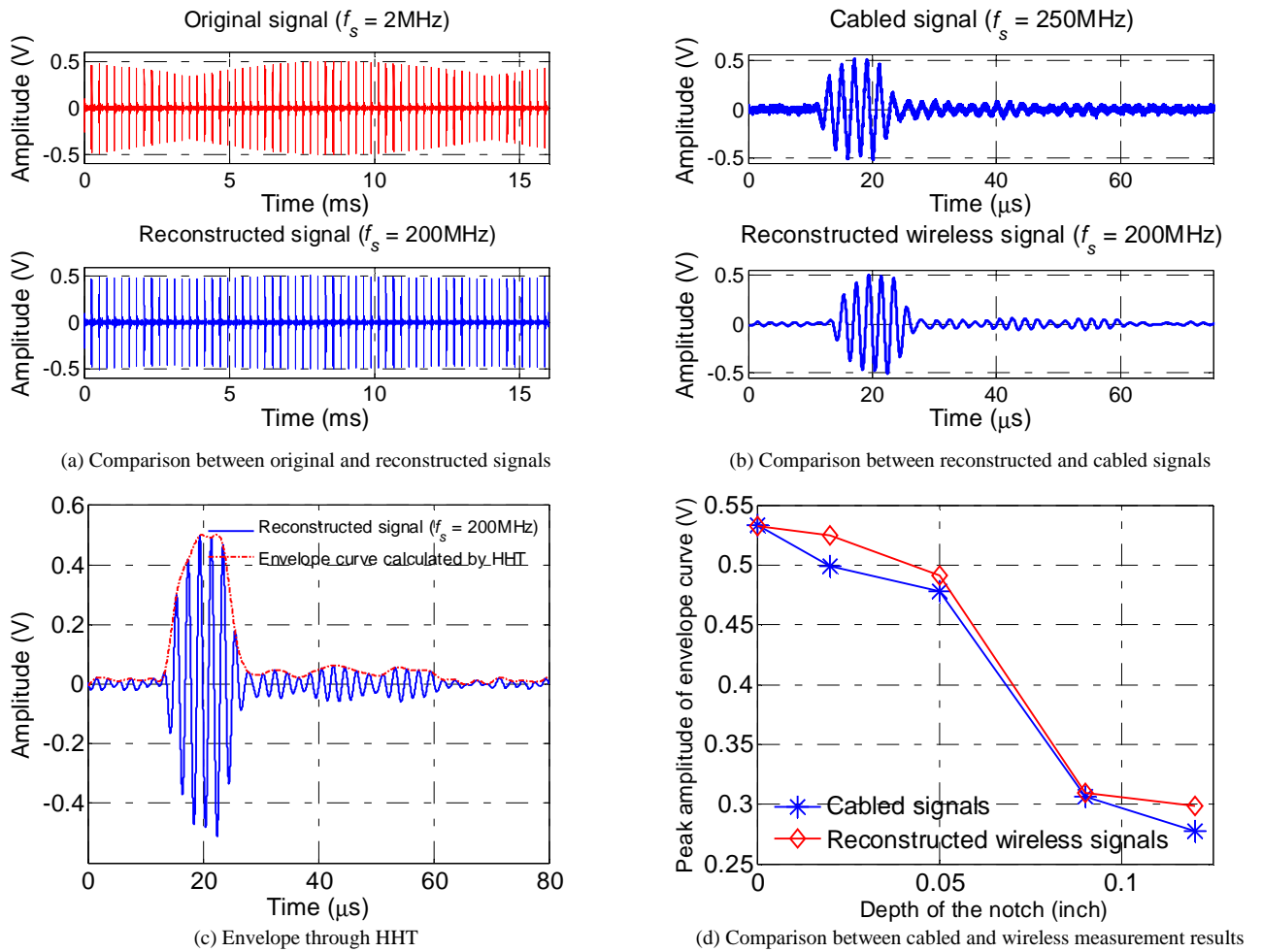(d) Comparison between cabled and wireless measurement results

Figure 13. Experiment results for the ultrasonic wing

In order to accurately quantify the amplitude of received signals, Hilbert–Huang transform (HHT) is selected to calculate the envelope of the reconstructed signal for each burst [19]. One example of the reconstructed signal (collected at undamaged position) and its envelope are shown in Figure 13(c). The diamond line in Figure 13(d) plots the peak envelope amplitude of the received signals with respect to the notch depth. For each notch depth, peak envelope amplitude is averaged from 60 bursts. The results indicated that the peak amplitude decreases when the notch depth increases. The asterisk line represents the results from the cabled data acquisition system. The trend is similar between the cabled and wireless system. The experiment demonstrates that measurement of the ultrasonic wing is sensitive to surface defects.

C. Validation of integrated accelerometer wing

To validate the performance of the integrated Martlet accelerometer wing, experiments are conducted on a four-story aluminum frame structure in the lab. Two integrated accelerometer wings are tested, each installed next to a high-precision cabled accelerometer (Silicon Designs 2012-002). One of the integrated accelerometer wings is installed at the base of the structure to measure the ground acceleration, and the other integrated accelerometer wing is installed at the first elevate slab to measure the structural response. A modal shaker is used to apply dynamic excitation to the structure (Figure 14). In the experiment, the amplification gain of the integrated accelerometer wings is set to ×20, and the cutoff frequency is set as 25Hz.

Figure 15 compares the time history data from the cabled accelerometers and the integrated accelerometer wings. The left two plots show the data over 10 seconds, and the right plots are close-up view of 3 seconds. All figures illustrate excellent agreement between the data sets collected by the wireless and cabled systems. Figure 15(b) particularly shows that the wireless time history data are almost indistinguishable to the cabled data. It is demonstrated that the integrated accelerometer wing is capable of providing high-quality acceleration measurements that are comparable with the cabled system in this test.
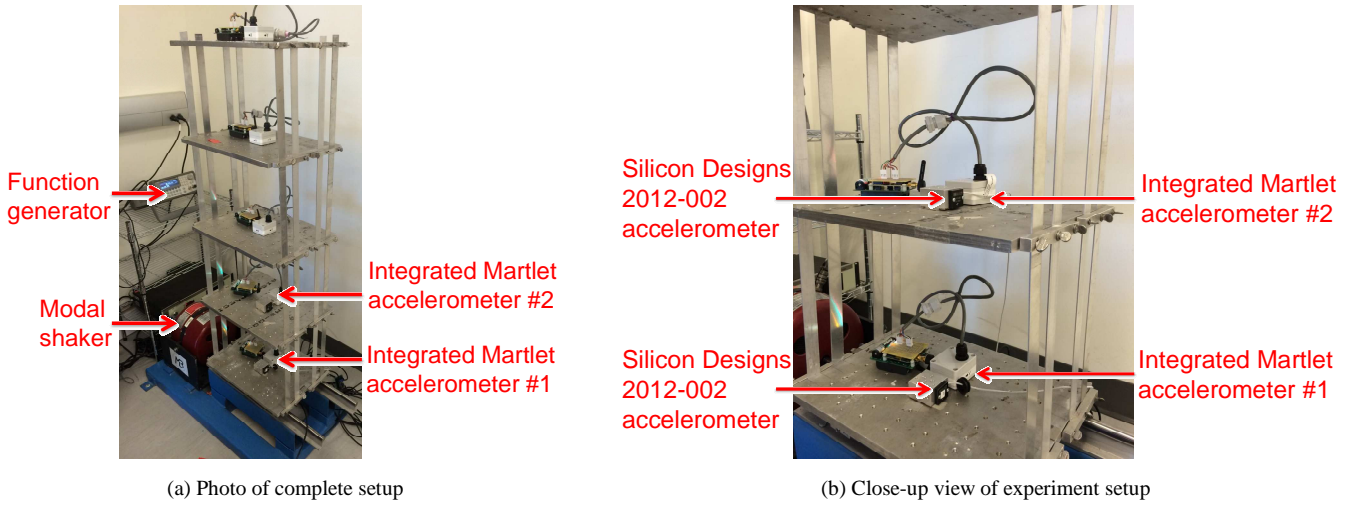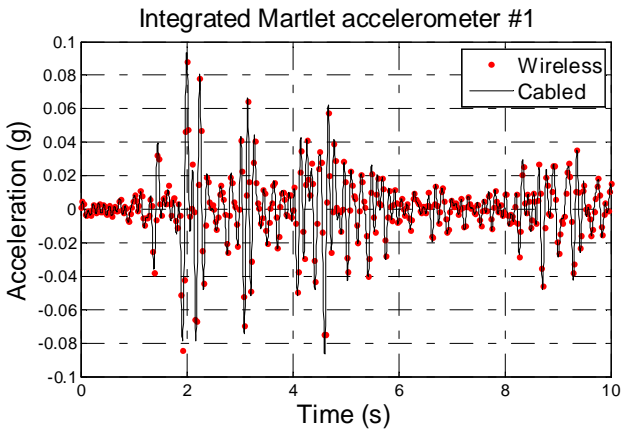
(a) Photo of complete setup

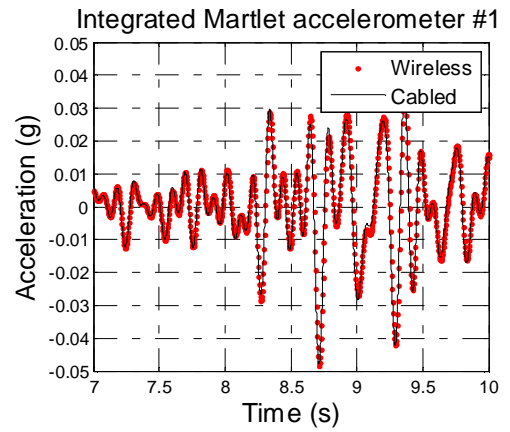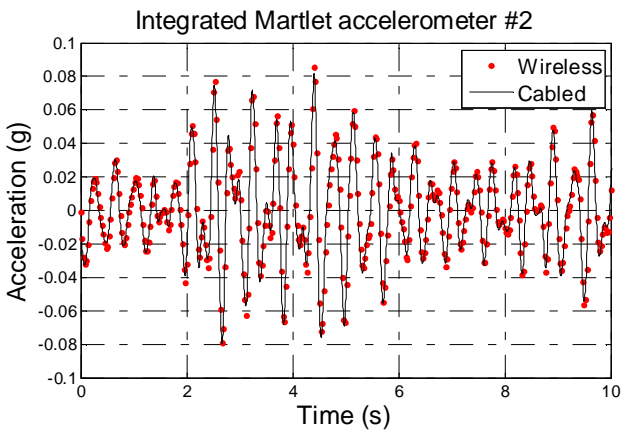

(b) Close-up view of experiment setup

Figure 14. Experiment setup for the integrated accelerometer wing
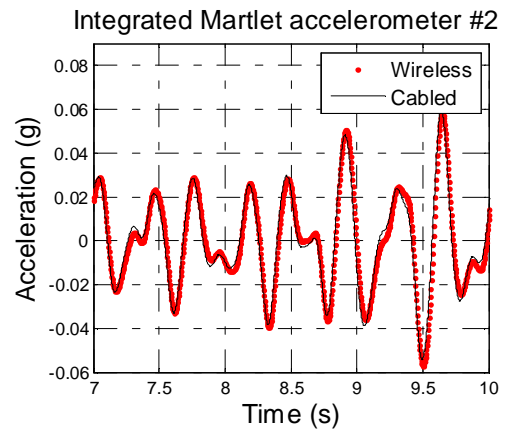

(a) Comparison for integrated Martlet accelerometer #1

(b) Close-up comparison for integrated Martlet accelerometer #1

(c) Comparison for integrated Martlet accelerometer #2

(d) Close-up comparison for integrated Martlet accelerometer #2

Figure 15. Comparison between integrated Martlet accelerometer wing and cabled accelerometer

IV. Summary and Discussion

This paper presents the latest development and validation of a next-generation, low-cost wireless sensing system for structural health monitoring, named Martlet. The Martlet node provides an extensible wireless platform which is able to execute high-frequency data acquisition and high-speed onboard computation. Standardized wing boards can be easily plugged in with the Martlet motherboard, which allows simultaneous data acquisition from multiple sensors of various types. In addition, the onboard Micro SD card significantly extends the data storage space of the Martlet node.

The newly-developed strain gage wing can provide strain measurement for 120Ω and 350Ω strain gages. The validation results demonstrate that the strain gage wing performs accurately and reliably in the calibration experiments and gives low noise level. In addition, the ultrasonic wing with 500 kHz ultrasonic transducers can help to detect defects in critical areas. The ultrasonic NDE results using a notched specimen demonstrate that the ultrasonic measurement is sensitive to the notch depth. Finally, the low-cost integrated accelerometer wing can provide accurate acceleration data measurement for dynamic testing. The amplification gain and cutoff frequency of the integrated accelerometer wings can be changed on the fly.

Future research will continue to improve the Martlet system in terms of power efficiency, reliability, and usability. More sensor wings can be developed for various needs in structural monitoring. Abundant applications in smart structures are yet to be discovered for the Martlet system.

References

[1] FHWA, "*National Bridge Inventory*," U.S. Department of Transportation, Federal Highway Administration, Washington D.C.2013.

[2] ASCE, *Report Card for America's Infrastructure*. Reston, VA: American Society of Civil Engineers, 2013.

[3] B. Jacob and V. Feypell-de La Beaumelle, "Improving truck safety: Potential of weigh-in-motion technology," *IATSS Research,* vol. 34, pp. 9-15, 2010.

[4] H. Zhao, N. Uddin, E. O'Brien, X. Shao, and P. Zhu, "Identification of vehicular axle weights with a Bridge Weigh-in-Motion system considering transverse distribution of wheel loads," *Journal of Bridge Engineering,* vol. 19, p. 04013008, 2014.

[5] C. W. Rowley, E. J. Obrien, A. Gonzalez, and A. Žnidarič, "Experimental testing of a moving force identification bridge weigh-in-motion algorithm," *Experimental Mechanics,* vol. 49, pp. 743-746, 2009.

[6] J. Herrmann, J.-Y. Kim, L. J. Jacobs, J. Qu, J. W. Littles, and M. F. Savage, "Assessment of material damage in a nickel-base superalloy using nonlinear Rayleigh surface waves," *Journal of Applied Physics,* vol. 99, p. 124913, 2006.

[7] S. K. Seth, S. M. Spearing, and S. Constantinos, "Damage detection in composite materials using Lamb wave methods," *Smart Materials and Structures,* vol. 11, p. 269, 2002.

[8] B. Peeters and C. E. Ventura, "Comparative study of modal analysis techniques for bridge dynamic characteristics," *Mechanical Systems and Signal Processing,* vol. 17, pp. 965-988, 2003.

[9] J. N. Juang and R. S. Pappa, "An eigensystem realization algorithm for modal parameter identification and modal reduction," *Journal of Guidance Control and Dynamics,* vol. 8, pp. 620-627, 1985.

[10] M. Celebi, "Real-time seismic monitoring of the new Cape Girardeau Bridge and preliminary analyses of recorded data: an overview," *Earthquake Spectra,* vol. 22, pp. 609-630, 2006.

[11] Y. Wang, J. P. Lynch, and K. H. Law, "Design of a low-power wireless structural monitoring system for collaborative computational algorithms," in *Proceedings of SPIE, Health Monitoring and Smart Nondestructive Evaluation of Structural and Biological Systems IV*, San Diego, CA, 2005

[12] T. Nagayama and B. F. Spencer, Jr., "*Structural health monitoring using smart sensors*," Newmark Structural Engineering Laboratory, University of Illinois at Urbana-Champaign, Urbana, IL Report No. NSEL-001, 2007.

[13] J. P. Lynch and K. J. Loh, "A summary review of wireless sensors and sensor networks for structural health monitoring," *The Shock and Vibration Digest,* vol. 38, pp. 91-128, 2006.

[14] R. A. Swartz, D. Jung, J. P. Lynch, Y. Wang, D. Shi, and M. P. Flynn, "Design of a wireless sensor for scalable distributed in-network computation in a structural health monitoring system," in *Proceedings of the 5th International Workshop on Structural Health Monitoring*, Stanford, CA, 2005

[15] M. Kane, D. Zhu, M. Hirose, X. Dong, B. Winter, M. Häckell*, et al.*, "Development of an extensible dual-core wireless sensing node for cyber-physical systems " in *Proceedings of SPIE, Sensors and Smart Structures Technologies for Civil, Mechanical, and Aerospace Systems*, San Diego, CA, USA, 2014

[16] T. Cooklev, *Wireless Communication Standards : a Study of IEEE 802.11, 802.15, and 802.16*. New York: Standards Information Network IEEE Press, 2004.

[17] A. Pertsch, J.-Y. Kim, Y. Wang, and L. J. Jacobs, "An intelligent stand-alone ultrasonic device for monitoring local structural damage: implementation and preliminary experiments," *Smart Materials and Structures,* vol. 20, p. 015022, 2011.

[18] P. Horowitz and W. Hill, *The Art of Electronics*, 2nd ed. Cambridge, England: Cambridge University Press, 1989.

[19] N. E. Huang, Z. Shen, S. R. Long, M. C. Wu, H. H. Shih, Q. Zheng*, et al.*, "The empirical mode decomposition and the Hilbert spectrum for nonlinear and non-stationary time series analysis," *Mathematical, Physical and Engineering Sciences,* vol. 454, pp. 903-995, 1998.